Integrated multi-omics profiling of plasma extracellular vesicles reveals the hsa-miR-1-3p-LRP1 axis as a potential biomarker in cervical cancer

TONGHUI BAO[1], XIAOPING LI[2], WUFEN LI[3], RUI YANG[4,5], YOUHONG YE[1], WENJIA ZHANG[1] and LIN QI[6]

[1]Department of Gynecology, Affiliated Hospital of Qinghai University, Xining, Qinghai 810000, P.R. China; [2]Department of Geriatrics, Affiliated Hospital of Qinghai University, Xining, Qinghai 810000, P.R. China; [3]Department of Hematology and Oncology, Qinghai Provincial Traditional Chinese Medicine Hospital, Xining, Qinghai 810000, P.R. China; [4]The Key Laboratory of Biomedical Information Engineering of Ministry of Education, School of Life Science and Technology, Xi'an Jiaotong University, Xi'an, Shaanxi 710000, P.R. China; [5]Bioinspired Engineering and Biomechanics Center, School of Life Science and Technology, Xi'an Jiaotong University, Xi'an, Shaanxi 710000, P.R. China; [6]Department of Oncology and Gynecology, Affiliated Hospital of Qinghai University, Xining, Qinghai 810000, P.R. China

Received June 23, 2025; Accepted December 12, 2025

DOI: 10.3892/mco.2025.2922

Abstract. Cervical cancer (CC) is a malignancy characterized by persistent human papillomavirus (HPV) infection, immune evasion and tumor microenvironment remodeling. Due to its high invasiveness and drug resistance, effective diagnosis and treatment remain challenging. The present study employed multi-omics analysis to explore the molecular characteristics of plasma extracellular vesicles (EVs) in CC. EVs were isolated from the plasma of 3 patients with CC and 3 healthy controls via ultracentrifugation, and validated by nanoparticle tracking analysis, transmission electron microscopy and western blotting. MicroRNA (miRNA or miR) sequencing identified 22 differentially expressed miRNAs, the target genes of which were enriched in HPV infection, p53, PI3K-Akt and Wnt signaling pathways. Proteomic analysis revealed 49 differentially expressed proteins associated with complement activation, cholesterol metabolism and coagulation. Integrated analysis highlighted key miRNA-protein interaction networks, identifying hsa-miR-1-3p and LRP1 as potential diagnostic biomarkers, and their differential expression was further confirmed by reverse transcription-quantitative PCR. These findings provide novel insights into the role of EVs in CC pathogenesis and offer promising potential targets for early diagnosis and therapeutic intervention.

Correspondence to: Dr Lin Qi, Department of Oncology and Gynecology, Affiliated Hospital of Qinghai University, 45 Tongren Road, Xining, Qinghai 810000, P.R. China
E-mail: kuyilaqlql@sina.com

Key words: cervical cancer, extracellular vesicles, transcriptomics, proteomics, integration analysis

Introduction

Cervical cancer (CC), one of the most prevalent malignancies of the female reproductive system worldwide, is primarily driven by persistent infection with high-risk human papillomavirus (HPV) (1). It is noteworthy that increasing evidence indicates that a subset of CC progresses through HPV-independent mechanisms, a process intricately linked to dynamic changes in the tumor microenvironment (TME) and complex intercellular communication (2,3). Currently, CC continues to pose important challenges in terms of drug resistance, precise diagnosis and effective treatment. Previous studies have shown that tumor heterogeneity and genomic instability can lead to resistance to chemotherapy and radiotherapy (4,5). Meanwhile, the infiltration of immunosuppressive cells, impaired T-cell function and upregulation of immune checkpoint molecules within the CC microenvironment collectively promote tumor immune evasion, thereby limiting the efficacy of immunotherapy (6,7). Furthermore, beyond anti-angiogenic agents, there remains a lack of effective targeted treatment strategies for metastatic or recurrent CC in clinical practice (8). However, current screening strategies and biomarker research for CC remain predominantly focused on HPV testing and cytological abnormalities. Although these methods can, to certain extent, predict disease progression and monitor treatment response, they exhibit notable limitations in accurately identifying precancerous lesions, addressing HPV-independent carcinogenic mechanisms, and monitoring treatment response and recurrence in patients with advanced-stage disease. Therefore, developing reliable biomarkers that can reflect TME alterations and disease evolution, and building more effective treatment strategies based on such biomarkers, has become a critical issue that urgently needs to be addressed in the clinical management of CC.

Extracellular vesicles (EV) have emerged as promising tools in liquid biopsy and tumor mechanism research due to their ability to carry various bioactive molecules such

as nucleic acids, proteins and metabolites (9). As a class of endogenous nanoparticles, EVs possess inherent characteristics, including low immunogenicity, high stability, and an exceptional ability to cross biological barriers, that make them ideal, universal platforms for cancer research and clinical application, far beyond a single cancer type (10). This broad utility is particularly evidenced in the field of biomarker discovery, where EV-based analyses have demonstrated significant diagnostic and prognostic value across a spectrum of malignancies, including breast, pancreatic and lung cancers (11,12). EVs are widely present in multiple biological fluids such as blood, saliva and urine (13-15). Among these, plasma holds particular value in EV research due to its easy accessibility, abundant availability, and capacity to rapidly and systematically reflect the body's pathophysiological status. EVs in plasma originate from tissues and organs throughout the body, including tumor tissues from different anatomical sites, enabling them to comprehensively reflect the body's tumor burden and heterogeneity (16,17). Building upon this universal potential of plasma EVs, their role in CC was investigated. During the development and progression of CC, plasma EVs are specifically regulated by the pathological state of CC cells, and their molecular composition carries disease-specific biological information (18). Therefore, analyzing the specific molecular characteristics of plasma EVs in the context of CC not only provides new perspectives for understanding the biological mechanisms of the disease, but also offers powerful tools for developing non-invasive diagnostic strategies.

At the molecular mechanism level, transcriptomics microRNA (miRNA or miR) sequencing has become a widely used approach for investigating cellular phenotypes and functions by deciphering upstream regulatory networks of gene expression (19,20). Specifically, miRNAs carried by EVs are not only protected from degradation but also functionally contribute to investigating the cause of disease, thus classifying cancer subtypes or acting as carriers targeting different target cells (12). They play important roles in a variety of cancer types and inflammatory diseases, including CC (21). However, transcriptomic analyses alone often fail to capture the multidimensional regulatory complexity of the disease due to inherent limitations in resolution and functional annotation. To overcome these limitations, proteomics offers a complementary and indispensable layer of information. As a downstream executor of gene expression, proteomic analysis provides detailed insights into post-translational modifications and functional protein interaction networks (22). This downstream perspective is critical for revealing the functional molecular mechanisms of diseases, identifying new biomarkers, and advancing personalized medicine. Building on the strengths of both fields, an integrated multi-omics strategy has emerged as a powerful paradigm. Indeed, previous studies have shown that integrating transcriptomics and corresponding proteomics data from EV samples cannot only reveal the association between genes and proteins, and explore the potential mechanisms of molecular networks, but also significantly enhance the identification of potential biomarkers for disease diagnosis (23,24). Consequently, monitoring circulating EV-derived miRNAs and proteins in body fluids offers a promising strategy for accurate, non-invasive and rapid disease diagnosis. Therefore, it was hypothesized that concurrently monitoring EV-derived miRNAs and proteins in plasma could provide a more accurate, non-invasive and comprehensive strategy for understanding CC pathogenesis and identifying diagnostic signatures.

In the present study, the aforementioned integrated multi-omics approach was employed to systematically reveal the molecular features and regulatory networks of plasma EV in CC progression. Combined analysis of EV miRNA transcriptomics and proteomics identified 22 differentially expressed miRNAs (DEMs) and 49 differentially expressed proteins (DEPs). These molecules were co-enriched in core pathways implicated in CC, including HPV infection, p53 signaling, PI3K-Akt pathway and complement/coagulation cascades. Notably, through multi-omics integration, the Homo sapiens (hsa)-miR-1-3p-LRP1 axis was identified and experimentally validated as a potential key regulatory target in CC. The present findings not only provide biological evidence supporting the use of plasma EVs as disease biomarkers, but also reveal novel signature molecules involved in CC onset and progression, thereby outlining a viable pathway for EV-mediated liquid biopsy and the development of targeted therapeutic strategies.

Materials and methods

Clinical samples. All participants were recruited from the Department of Gynecology, Qinghai University Affiliated Hospital (Qinghai, China). The cohort included 3 female patients with CC and 3 female healthy controls (HCs). The ages of the patients with CC were 44, 47 and 69 years (median: 53 years; range: 44-69 years), while the HCs were 58, 61, and 61 years old (median: 61 years; range: 58-61 years). This sample size aligns with standard practices for exploratory analysis using omics technologies and meets the requirements for methodological reproducibility (25,26). The present study was approved by the Institutional Review Board of Qinghai University Affiliated Hospital (approval no. P-SL-202157) in compliance with ethical standards, and written informed consent was obtained from all participants prior to enrollment. CC diagnoses were pathologically confirmed according to the International Federation of Gynecology and Obstetrics (FIGO) staging system (2018) (27). Venous blood samples were collected immediately after admission. Plasma was separated by centrifugation at 4˚C and 1,000 x g for 15 min (cat. no. HT165; Cence; https://www.xiangyilxj.com/) and stored at -80˚C until further analysis.

EV preparation. EV were isolated from 2 ml plasma using a standardized ultracentrifugation (UC) protocol (28). Briefly, plasma samples were diluted 10-fold with PBS (cat. no. G4202; Wuhan Servicebio Technology Co., Ltd.) to a final volume of 20 ml. Sequential centrifugation steps were then performed at 2,000 x g for 10 min at 4˚C to eliminate cellular debris and at 10,000 x g for 20 min at 4˚C to pellet larger apoptotic bodies, and filtered through a 0.22-μm pore-size membrane filter (cat. no. SLGP033R; MilliporeSigma) to remove large particulate contaminants. The supernatant was subsequently ultracentrifuged at 120,000 x g for 120 min at 4˚C (cat. no. OPTIMA L100XP; Beckman Coulter, Inc.) to obtain

purified EV pellets, which were resuspended in 400 μl sterile PBS and stored at -80˚C until further analysis.

Nanoparticle tracking analysis (NTA). NTA was performed using a NanoSight NS300 system (Malvern Panalytical, Ltd.) equipped with a 488-nm laser and a high-sensitivity sCMOS (scientific complementary metal-oxide-semiconductor) camera, according to the manufacturer's instructions. The samples were then diluted with PBS to achieve an optimal concentration for accurate particle counting and sizing, resulting in a final concentration of 30-50 particles per frame. The particles per frame value was 30-60, with a camera detection threshold of 15 and an automated injection flow rate of 30 μl/min.

Transmission electron microscope (TEM) analysis. After fixation with an equal volume of 4% paraformaldehyde (cat. no. BL539A; Biosharp Life Sciences) at 4˚C for 30 min, the EV suspension was deposited onto Formvar/carbon-coated copper grids (cat. no. BZ11032b; Henan Zhongjingkeyi Technology Co., Ltd.) and allowed to adsorb for 30 min at room temperature (RT). The grids were then washed twice with PBS, followed by post-fixation with 1% glutaraldehyde for 5 min. After two washes with ultrapure water, the samples were negatively stained with 2% uranyl acetate (cat. no. GZ02625, Tianjin Ruixin Technology Co., Ltd.) at RT for 40 sec. Morphological observation was ultimately performed using a Talos L120C G2 TEM (Thermo Fisher Scientific, Inc.) operated at 120 kV.

Western blot (WB) analysis. Purified EVs were quantified using a the Bicinchoninic Acid Assay Kit (BCA; cat. no. P0011; Beyotime Institute of Biotechnology) according to the manufacturer's instructions. Deformed EV proteins (loaded with 20 μg of protein per lane) were separated by 10% SDS-PAGE using the One-Step PAGE Gel Rapid Preparation Kit (cat. no. PG212; Shanghai Epizyme Biopharmaceutical Technology Co., Ltd.; Ipsen Pharma) and transferred to a PVDF membrane (cat. no. ISEQ00010; MilliporeSigma). Membranes were blocked with 5% (w/v) non-fat milk (cat. no. 232100; Sangon Biotech Co., Ltd.) in PBS containing 0.1% Tween-20 (cat. no. 30189380; Shanghai HUSHI, Ltd.) for 1 h at RT and subsequently incubated overnight at 4˚C with the following primary antibodies diluted in blocking buffer: Anti-Alix (1:1,000; cat. no. 18269; Cell Signaling Technology, Inc.), anti-Flotillin-1 (1:1,000; cat. no. 610820; BD Biosciences) and anti-CD63 (1:1,000; cat. no. ab68418; Abcam). After five washes with PBS, membranes were incubated with a horseradish peroxidase conjugated goat anti-rabbit IgG secondary antibody (1:3,000; cat. no. 7074; Cell Signaling Technology, Inc.) for 1 h at RT. Protein bands were visualized using a ChemiDoc Imaging System (Clinx Science Instruments, Co., Ltd.) with an enhanced chemiluminescence substrate (cat. no. WBKLS0500; MilliporeSigma).

miRNA sequencing and bioinformatic analysis. Total RNA was extracted from purified EV using RNAiso for miRNA reagent (cat. no. 9753A, Takara Bio, Inc.), a specialized reagent designed for the simultaneous isolation of both large and small RNAs. RNA concentration and purity were assessed using a NanoDrop One spectrophotometer (cat. no. 840-317400; NanoDrop Technologies; Thermo Fisher Scientific, Inc.). Briefly, EV samples were thoroughly mixed with 140 μl chloroform (cat. no. C2432; MilliporeSigma) and centrifuged at 12,000 x g for 15 min at 4˚C. The aqueous phase was collected and combined with 1.5 vol absolute ethanol. The mixture was transferred to RNeasy purification columns (cat. no. 74104; Qiagen GmbH) for RNA purification. Small RNA libraries were constructed from 1 μg of total RNA per sample. Subsequently, 4 μl miRNA was subjected to 18 cycles of microamplification using the SMARTer® Starfish Total RNA-seq Kit (cat. no. 634413; Takara Bio, Inc.), and the amplified products were purified with AMPure XP beads (cat. no. A63881; Beckman Coulter, Inc.). Libraries were then constructed from 1 ng complementary DNA (cDNA) using the Transpose DNA Library Prep Kit for Illumina, Inc. (cat. no. K0012; LifeInt) with 14 amplification cycles. The final libraries were quality-controlled on an Agilent 2100 Bioanalyzer (cat. no. G2939A; Agilent Technologies, Inc.) to ensure a peak distribution between 140-160 bp, corresponding to miRNA inserts, and sequenced on an Illumina NovaSeq 6000 platform (Illumina, Inc.), generating paired-end 150-bp reads from six samples.

For bioinformatic analysis, raw sequencing data were processed with Trim Galore (v0.6.7; The Babraham Institute) to remove adapter sequences and low-quality reads (Phred quality score <30). High-quality reads were aligned to the human reference genome GRCh38/hg38 using Bowtie2 (v2.4.5). miRNA expression quantification was performed with miRDeep2 (v2.0.1.3) to calculate read counts, and miRNAs with null expression in ≥50% of samples were filtered out. DEMs were identified using DESeq2 (v1.32.0) with thresholds of fold-change (FC) >1.2 and adjusted $P<0.05$. miRNA target genes were predicted based on the miRTarBase database (v9.0; https://mirtarbase.cuhk.edu.cn/~miRTarBase/miRTarBase_2022/php/index.php). Gene Ontology (GO) and Kyoto Encyclopedia of Genes and Genomes (KEGG) pathway enrichment analyses were conducted using ClusterProfiler (v4.2.2) (29), which is available from Bioconductor (https://bioconductor.org/packages/clusterProfiler/). A significance threshold of $P<0.05$ was applied. The results were visualized with ggplot2 (v3.3.5).

Proteomic profiling and bioinformatic analysis. EV samples were thawed at -80˚C and lysed on ice with 1% (v/v) protease inhibitor cocktail using ultrasonication. The lysate was centrifuged at 12,000 x g for 10 min at 4˚C to remove cellular debris, and the supernatant was transferred to fresh microcentrifuge tubes. Protein concentration was quantified using a BCA assay kit (cat. no. P0011; Beyotime Institute of Biotechnology). For each sample, 50 μg EV protein was adjusted to 100 μl with lysis buffer. Proteins were reduced with 5 mM dithiothreitol (cat. no. 43815; MilliporeSigma) at 56˚C for 30 min, followed by alkylation with 11 mM iodoacetamide (cat. no. I1149; MilliporeSigma) in the dark at RT for 15 min. Urea concentration was diluted to <2 M using tetraethylammonium bromide. Sequential tryptic digestion was performed with trypsin. Peptides were reconstituted in 0.1% formic acid (FA: cat. no. 94318; MilliporeSigma) and separated

Table I. Primer sequences.

Primer	Sequence (5'-3')	Note
hsa-miR-1-3p	F: TGGAATGTAAAGAAGTATGTAT	Targets the mature miR-1-3p sequence
	R: GTGCAGGGTCCGAGGT	Universal reverse primer
LRP1	F: CTATCGACGCCCCTAAGACTT	
	R: CATCGCTGGGCCTTACTCT	
GAPDH	TGTGGGCATCAATGGATTTGG	
	ACACCATGTATTCCGGGTCAAT	

F, forward; R, reverse; miR, microRNA.

on an EASY-nLC 1200 UHPLC system (Thermo Fisher Scientific, Inc.). The mobile phases consisted of 0.1% FA + 2% acetonitrile (ACN; phase A) and 0.1% FA + 90% ACN (phase B). The gradient program was: 0-68 min (6-23% B), 68-82 min (23-32% B), 82-86 min (32-80% B) and 86-90 min (80% B) at a flow rate of 500 nl/min. Peptides were ionized via a nano-electrospray ionization source and analyzed on an Orbitrap Exploris™ 480 mass spectrometer. The ion source voltage was set to 2.3 kV. FAIMS compensation voltages were configured at 45 and -65 V. High-resolution Orbitrap detection was applied for both precursor (400-1,200 m/z; 60,000 resolution) and fragment ions (fixed start at 110 m/z; 15,000 resolution), with TurboTMT disabled. Data-dependent acquisition mode was used to select the top 25 most intense precursors per cycle for fragmentation (AGC target 100%, signal threshold $5x10^4$ ions/sec). Raw data were processed through Proteome Discoverer (v2.4.1.15) against the UniProt human proteome database (Homo_SP_20201214.fasta; 20,395 sequences). Screening thresholds for differential proteins were as follows: FC>1.5 and P<0.05. Protein-protein interaction (PPI) networks were analyzed using the STRING database (v11.5; https://cn.string-db.org/; confidence level >0.9) and visualized using Cytoscape (v3.10.3). Functional enrichment analysis was conducted using ClusterProfiler (v4.2.2), and the results were visualized with ggplot2 (v3.3.5). Tissue localization of EV proteins was inferred by mapping expression profiles to immunohistochemical data from the Human Protein Atlas (https://www.proteinatlas.org).

Integrative analysis of DEMs and proteomics. The co-expression associations between DEMs and DEPs were evaluated using Spearman's correlation coefficient, and were visualized via heatmaps (v1.0.12). By integrating KEGG pathway annotations of DEM target genes and DEPs, pathways significantly enriched in both omics datasets were identified. Overlapping pathways were illustrated using Venn diagrams (v1.6.20), available on CRAN (https://cran.r-project.org/package=VennDiagram) (30). Functional prioritization of shared pathways was performed based on enrichment factor and gene/protein coverage. From the miRNA-protein co-expression network, highly dense functional modules were extracted using the MCODE plugin (Cytoscape, v2.0.0; https://apps.cytoscape.org/apps/mcode). Core regulatory hubs were identified via the Degree algorithm in the CytoHubba plugin (Cytoscape, v0.1), which were defined as molecules with the highest topological centrality.

Reverse transcription-quantitative PCR (RT-qPCR). Following plasma EV extraction from the HC and CC groups, total RNA was isolated according to the manufacturer's protocol of TRIzol™ reagent (cat. no. 15596026; Invitrogen; Thermo Fisher Scientific, Inc.). The key steps included lysing the sample in TRIzol™, followed by 5-min incubation at RT, addition of chloroform (cat. no. C2432; MilliporeSigma), centrifugation to separate the phases, collection of the aqueous phase, precipitation of RNA with isopropanol (cat. no. 34863; MilliporeSigma), two washes with 75% ethanol, air-drying and resuspension of the RNA pellet in DEPC-treated water. RNA concentration and purity were assessed using a NanoDrop spectrophotometer. For RT, LRP1 mRNA was transcribed using the PrimeScript™ RT Kit (cat. no. RR047; Takara Bio, Inc.) with 1 μg total RNA as a template, and the product was diluted 5-fold for later use. To ensure specific detection of mature hsa-miR-1-3p, a targeted stem-loop RT primer was used for RT. qPCR was then performed using the SYBR Green Premix (cat. no. AG11701; Hunan Accurate Bio-Medical Technology Co., Ltd.), which was selected for its cost-effectiveness and compatibility with simultaneous detection of both miRNA and mRNA targets, with a reaction volume of 20 μl, including 2 μl diluted cDNA, 0.8 μl forward and reverse primers (10 μM), 10 μl pre-mixed SYBR Green Premix, and 6.4 μl ddH_2O. The program was set to 95˚C pre-denaturation for 1 min, followed by 45 cycles of 94˚C for 20 sec and 58˚C for 30 sec. Melting curve analysis was systematically performed to verify amplification specificity (LineGene 9600 Plus; Hangzhou Bioer Co., Ltd.). All samples were analyzed in triplicate wells with blank controls, and relative expression levels were calculated using the $2^{-\Delta\Delta Cq}$ method (31). The internal references were GAPDH (for LRP1) and U6 (for miR-1-3p). The primer sequences are shown in Table I.

Statistical analysis. Graphical and statistical analyses were performed using the ggplot2 package (v3.3.5), GraphPad Prism (v8.0.12; GraphPad; Dotmatics) and Cytoscape software (v3.10.2). Data from three independent experiments are presented as the mean ± standard deviation. Statistical comparisons between the HC and CC groups were performed using an unpaired, two-tailed Student's t-test. P<0.05 was considered to indicate a statistically significant difference.

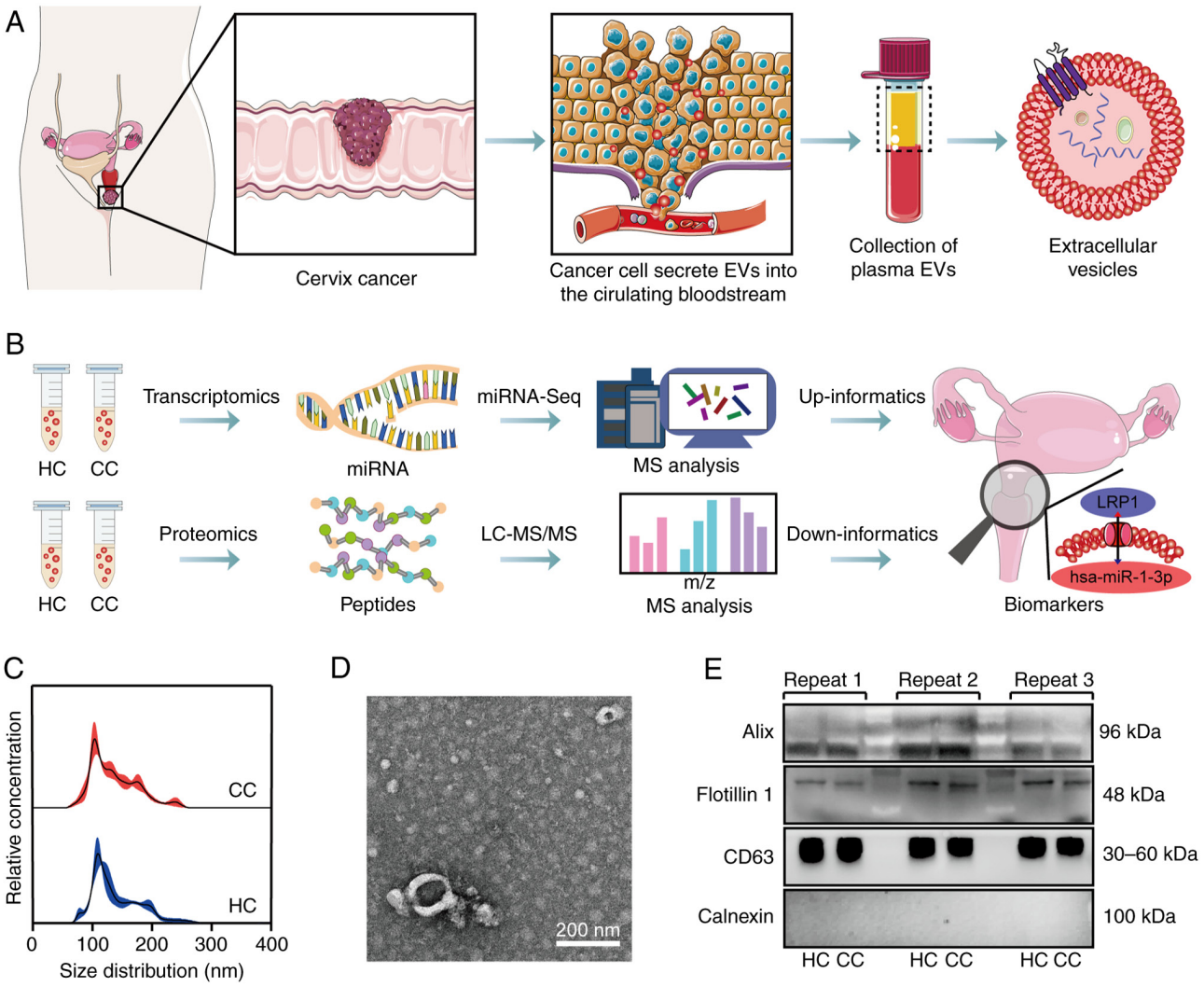

Figure 1. Isolation and characterization of plasma-derived EVs from patients with CC and HC. (A) Overall experimental design for CC plasma EV isolation. (B) Workflow of analytical strategies for miRNA sequencing, proteomics and multi-omics integration. (C) Nanoparticle tracking analysis revealed the size distribution of plasma EV. (D) Transmission of EV electron microscopy images. (E) Western blot validation of EV markers. EVs, extracellular vesicles; CC, cervical cancer; HC, healthy controls; miR or miRNA, microRNA; LC-MS, Liquid chromatography-mass spectrometry.

Results and Discussion

EV isolation and characterization from plasma samples. The present study included a total of 6 plasma samples, comprising 3 patients with CC and 3 HCs. CC diagnosis was confirmed according to the 2018 FIGO staging criteria (32), supplemented by imaging, molecular pathology, and histopathological biopsy results. The overall experimental workflow is revealed in Fig. 1A, while the analytical pipeline for miRNA transcriptomics, proteomics and multi-omics integration is outlined in Fig. 1B. EVs were isolated from plasma using UC. NTA showed EV sizes predominantly ranging from 50-200 nm, with peak sizes of 105 nm (CC) and 111 nm (HC) (Fig. 1C). No significant intergroup differences were observed in particle size distribution or concentration (~$1.5x10^{10}$ particles/ml). TEM imaging demonstrated EV exhibiting typical cup-shaped or biconcave discoid morphology (Fig. 1D). Following the MISEV2018 guidelines (33), WB analysis confirmed EV' purity, demonstrating consistent expression of positive markers (Alix, Flotillin-1 and CD63) and absence of calnexin contamination (20 μg protein load; Fig. 1E). Semi-quantitative analysis showed stable marker expression without significant differences between the HC and CC groups (Fig. S1A-C).

Differential expression and functional implications of EV-derived miRNAs in CC. miRNA sequencing identified 2,656 miRNAs, with 22 DEMs (9 upregulated and 13 downregulated in CC) using DESeq2 (FC >1.2, P<0.05; Fig. 2A). Hierarchical clustering showed distinct disease-specific expression profiles (Fig. 2B). To further investigate the biological functions of these DEMs, their target genes were predicted using the miRTarBase database. These predicted targets were then subjected to KEGG and GO enrichment analyses. KEGG analysis showed that DEM targets were significantly enriched in several key cancer-related pathways, including the p53 signaling pathway, PI3K-Akt signaling pathway, Wnt signaling pathway, focal adhesion and HPV infection (Fig. 2C). These pathways are critically involved in HPV-associated oncogenesis, immune evasion mechanisms, chemoresistance and TME signaling (34,35). GO enrichment

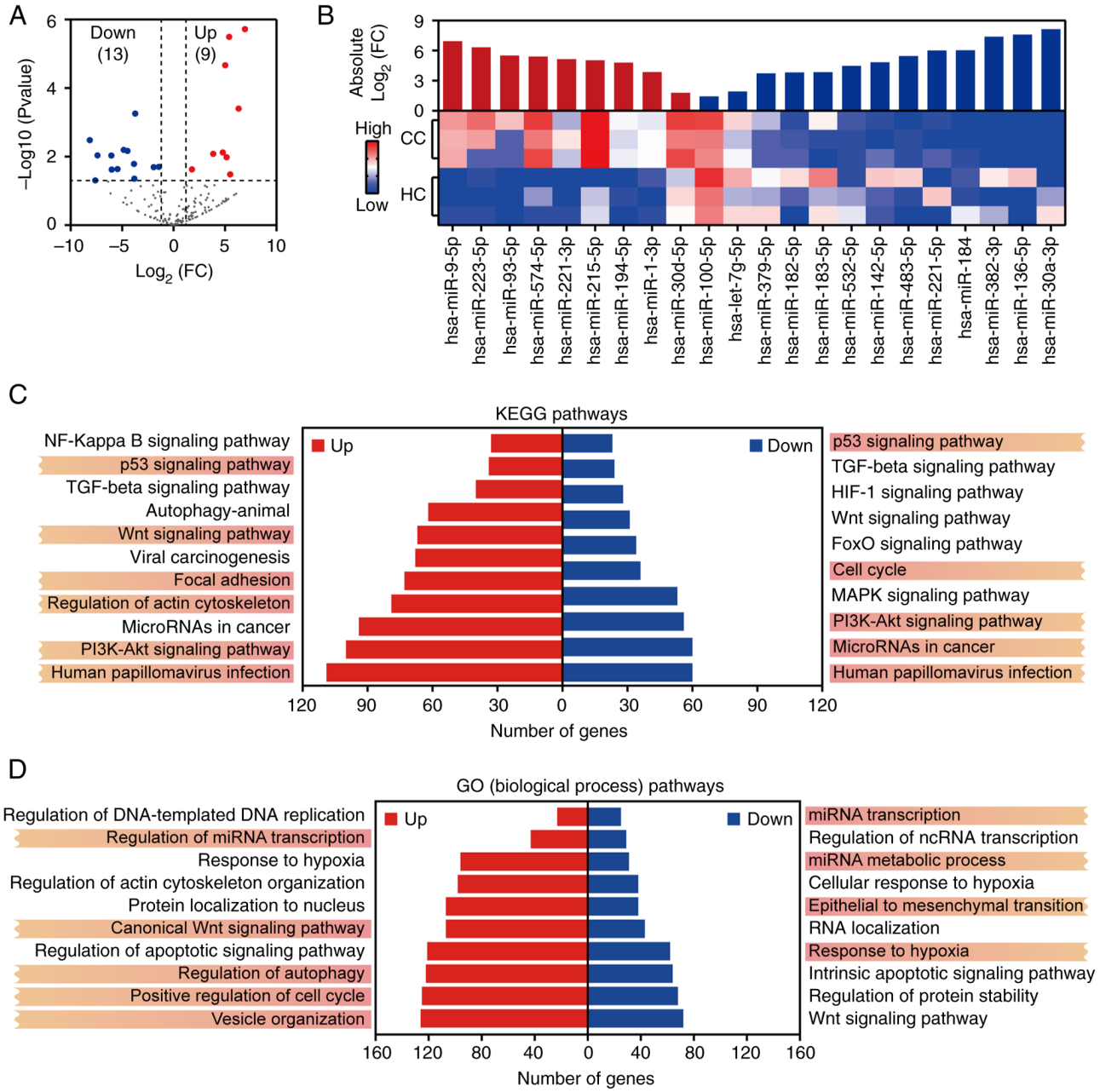

Figure 2. Differential expression and functional enrichment analysis of extracellular vesicle-derived miRNAs in CC. (A) Volcano plot showing DEMs between patients with CC and HC. (B) Heatmap and corresponding bar chart of DEMs in CC and HC groups. (C) KEGG pathway enrichment analysis of predicted target genes of DEMs. (D) GO enrichment analysis of DEMs target genes. miR or miRNA, microRNA; CC, cervical cancer; DEMs, differentially expressed miRNAs; HC, healthy controls; KEGG, Kyoto Encyclopedia of Genes and Genomes; GO, Gene Ontology.

analysis further revealed that these miRNAs were involved in biological processes such as regulation of miRNA transcription, canonical Wnt signaling pathway, vesicle organization, regulation of autophagy and positive regulation of the cell cycle (Fig. 2D). Collectively, these findings suggest that EV-derived miRNAs may contribute to CC progression through multiple functional modules, including HPV-induced cell cycle dysregulation, EV-mediated tumor-stroma communication and stress response regulation (36,37).

Specific miRNA-pathway interactions were further investigated. The target genes of miR-221-3p and miR-182-5p were significantly enriched in HPV infection and PI3K-Akt signaling, while hsa-miR-30a-3p and hsa-miR-194-5p were enriched in p53 signaling. This suggests that EV-derived miRNAs may synergize with viral oncoproteins to remodel oncogenic signaling networks and promote chemoresistance. For example, miR-30a-3p may enhance chemoresistance by inhibiting downstream targets of p53 (38). This indicates that EV miRNAs may act as amplifiers of HPV oncogenesis and promote tumor heterogeneity through intercellular communication; thus, targeting these miRNAs may reverse chemoresistance. Furthermore, the enrichment of DEM target genes in positive regulation of the cell cycle, vesicle organization, miRNA transcription and regulation of actin cytoskeleton organization pathways likely contributes to CC proliferation and invasion. Specifically, hsa-miR-221-3p

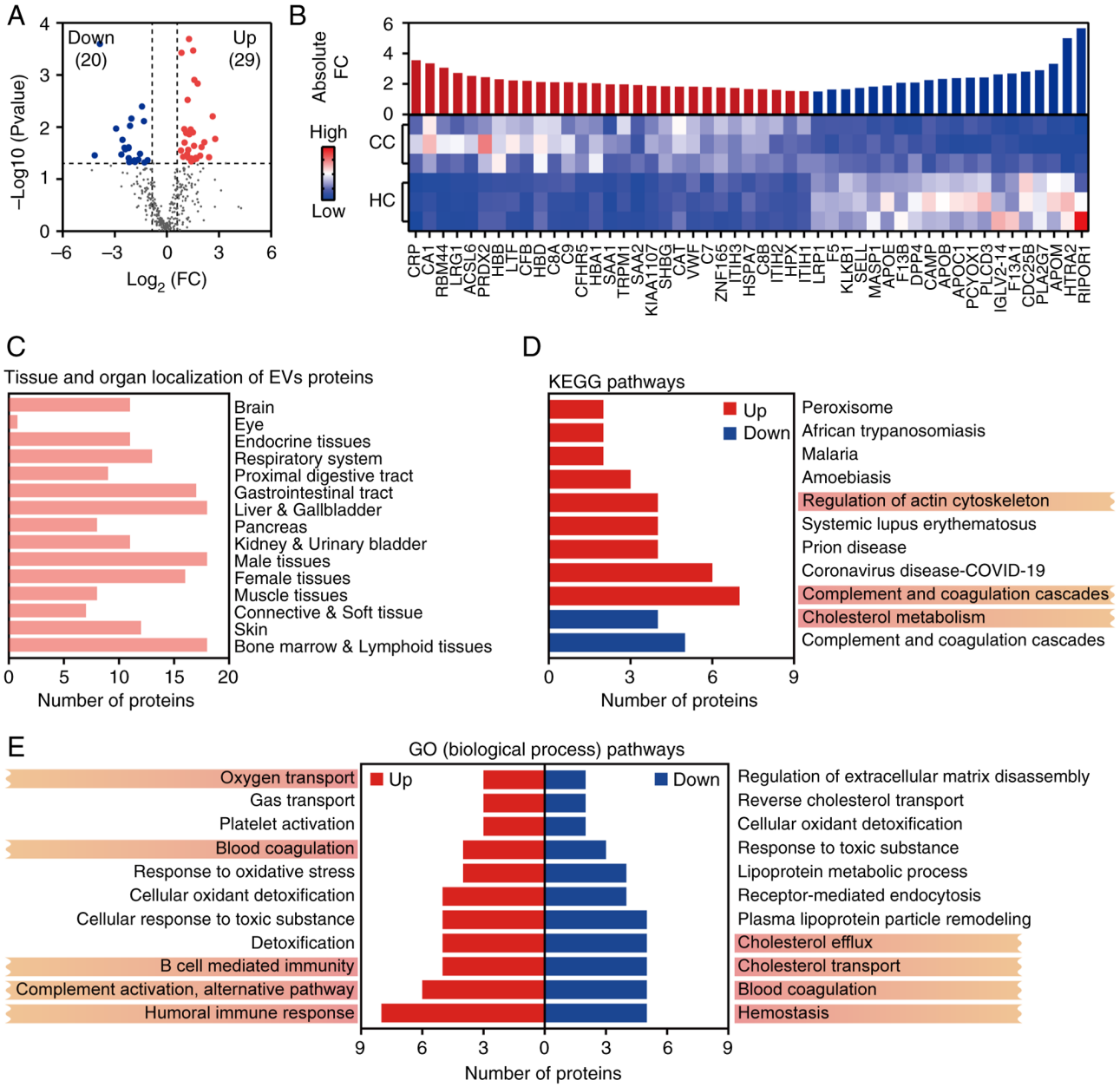

Figure 3. Proteomic profiling and functional enrichment analysis of plasma-derived extracellular vesicles in CC. (A) Volcano plot of DEPs between HC and patients with CC. (B) Heatmap and corresponding bar plot of DEPs in CC and HC groups. (C) Tissue and organ distribution of EV-derived DEPs. (D) KEGG pathway enrichment analysis of DEPs. (E) GO pathway enrichment analysis of DEPs. CC, cervical cancer; DEPs, differentially expressed proteins; HC, healthy controls; KEGG, Kyoto Encyclopedia of Genes and Genomes; GO, Gene Ontology.

and hsa-miR-30d-5p both target CASP3, a key regulator of apoptosis and tumor cytotoxicity (39), which may influence apoptotic processes. Additionally, hsa-miR-221-3p may affect transcription factor activity (40). hsa-miR-9-5p and hsa-miR-93-5p were associated with miRNA transcription, suggesting their potential involvement in epigenetic feedback loops that drive tumor heterogeneity (41,42).

Proteomic profiling of EV reveals immune, metabolic and coagulation signatures in CC. Proteomic analysis identified 363 EV-associated proteins, with 49 DEPs (29 upregulated and 20 downregulated) using limma (FC >1.5, P<0.05; Fig. 3A). Hierarchical clustering revealed disease-specific protein signatures (Fig. 3B). Tissue origin analysis indicated that DEPs were primarily derived from the liver, gallbladder, female reproductive organs and gastrointestinal tract (Fig. 3C). This tissue-specific distribution highlights EVs as promising biomarkers for reflecting pathophysiological alterations, particularly in reproductive and digestive system-related malignancies. To explore the functional roles of these DEPs, GO and KEGG enrichment analyses were conducted. KEGG pathway analysis showed significant enrichment of DEPs in the complement and coagulation cascades, regulation of actin cytoskeleton, and cholesterol metabolism pathways (Fig. 3D). GO enrichment further identified DEP involvement in complement activation, the alternative complement pathway, blood coagulation and lipopolysaccharide (LPS)-mediated signaling (Fig. 3E). These pathways may collectively drive CC

progression by modulating immunosuppressive TMEs, thus enhancing cell motility and invasion, and facilitating HPV genome integration.

Previous studies have shown that HPV-infection tumor cells can escape immune escape by inhibiting the activity of natural killer and T cells (43). The present findings further support this mechanism, as multiple complement-related proteins (including C5, C7, C8A/B, C9 and CFB) were significantly upregulated in CC-EV and enriched in the alternative complement activation pathway (44,45). These observations align with previous research suggesting that EV contribute to immunosuppressive environments via complement system modulation (46). Additionally, inflammatory mediators such as CRP and SAA1/2 were highly expressed and mapped to pathways related to LPS signaling and acute inflammatory responses (47,48). These proteins may contribute to an inflammatory microenvironment that supports persistent HPV infection and tumor progression. EVs also carry elevated levels of antioxidant enzymes, including catalase and peroxiredoxin-2, which are known to neutralize reactive oxygen species and maintain redox balance, thereby preserving tumor cell viability under oxidative stress (49,50). Lipid metabolism-related proteins, such as APOE, APOB and APOC1, were significantly enriched in the cholesterol metabolism pathway, while pattern recognition receptors such as TLR4 were involved in activating the NF-κB pathway. For example, overexpression of APOE in EVs may enhance CC cell invasion via the PI3K-Akt signaling pathway (51). This suggests that EV act as molecular hubs integrating metabolic reprogramming and inflammatory signaling to support a tumor-permissive microenvironment and sustain malignant transformation. In the current study, aberrant expression of F5, F13A1 and F13B was observed. These coagulation factors, which are involved in pathways such as blood coagulation and platelet activation, may be associated with CC angiogenesis and metastasis. Collectively, these specific protein signatures offer promising targets for EV-based liquid biopsy, and may provide new avenues for mechanistic studies and therapeutic intervention in CC.

Integrated multi-omics analysis reveals a key miRNA-protein regulatory axis in CC-EV. To systematically dissect the molecular regulatory network mediated by EV in CC, an integrative analysis combining EV-derived miRNA expression profiles and proteomic data was performed. This multidimensional approach aimed to identify key regulatory axes and diagnostic biomarkers. Spearman correlation analysis revealed significant positive and negative associations between DEMs and DEPs, suggesting that EV-contained miRNAs may regulate downstream protein expression via direct targeting (Fig. 4A). Pathway enrichment analysis of co-expressed DEMs and DEPs demonstrated convergence in three major biological pathways, namely regulation of the actin cytoskeleton, prion disease and coronavirus disease-19 (Fig. 4B). These results suggested that dysregulated EV-derived miRNAs may modulate cytoskeletal remodeling, influence viral or misfolded protein handling, and shape inflammatory responses within the TME. Notably, targeting of the actin cytoskeleton regulator LRP1 by EV miRNAs suggests a mechanistic link to enhanced CC cell motility and invasiveness (52,53).

To further investigate protein-level regulatory hubs, PPI network analysis identified APOE, CRP and APOB, which are lipid metabolism-related proteins, as central nodes among DEPs (Fig. 4C), thus highlighting lipid metabolic reprogramming as a major driver of CC-associated EV signaling. Cross-referencing this network with miRNA-protein interactions revealed that hsa-miR-1-3p was the only miRNA directly connected to multiple hub proteins, including LRP1, FN1, C8A and PDLIM7 (Fig. 4D). Notably, tissue-specific expression analysis showed that LRP1 was highly expressed in female reproductive tissues, including the endometrium, ovary and breast (Fig. 4E), thus underscoring its relevance in gynecological malignancies. Previous research has shown that hsa-miR-1-3p promotes non-small cell lung cancer progression by participating in mechanosensitive mitotic processes (54), while activation of LRP1 fucosylation suppresses epithelial-mesenchymal transition (EMT) and metastasis in CC (55). In the present study, hsa-miR-1-3p was significantly upregulated in EV from patients with CC, whereas LRP1 was significantly downregulated (Fig. 4F), suggesting that this miRNA may inhibit LRP1 expression to drive CC pathogenesis. These findings indicate that elevated hsa-miR-1-3p in EV may inhibit LRP1-mediated inflammatory chemotaxis, increase oxidative stress within the TME, and activate Wnt/β-catenin signaling to promote EMT. Such a mechanism aligns with previously described roles of EV-carried miRNAs in tumor metastasis, and highlights the hsa-miR-1-3p-LRP1 axis as a potential diagnostic and therapeutic target (56). In summary, this integrative multi-omics analysis uncovered a key EV-derived miRNA-protein regulatory circuit in CC, providing novel insights into disease progression and supporting the clinical utility of hsa-miR-1-3p and LRP1 as candidate biomarkers for EV-based liquid biopsy in CC.

Through integrated analysis of miRNA transcriptomics and proteomics from plasma EV of HCs and patients with CC, the present study unveiled a complex molecular regulatory network during CC progression, which not only confirmed the potential of EV as disease biomarkers, but, more importantly, revealed that upregulated hsa-miR-1-3p in CC may participate in disease progression by suppressing LRP1 expression.

The current study has demonstrated that plasma-derived EV from patients with CC undergo marked alterations in both miRNA and protein composition. The identified DEMs and their predicted target genes were significantly enriched in classical CC-related pathways such as p53 and PI3K-Akt (57,58). Notably, through multi-omics integration analysis of plasma EV, it was identified that activity changes in these pathways could be carried and transmitted by EV. For instance, miR-221-3p and miR-182-5p may simultaneously affect both HPV infection and the PI3K-Akt signaling pathway, indicating that EV miRNAs may serve as 'regulatory nodes' coordinating the cross-talk between different carcinogenic pathways, thereby amplifying the oncogenic effects of HPV viral oncoproteins (59-62). At the protein level, the present study revealed significant enrichment of complement and coagulation cascades, suggesting that tumor-derived EV may shape an immunosuppressive TME by modulating the innate immune and coagulation systems, thus promoting immune escape and angiogenesis (63,64). Meanwhile, the

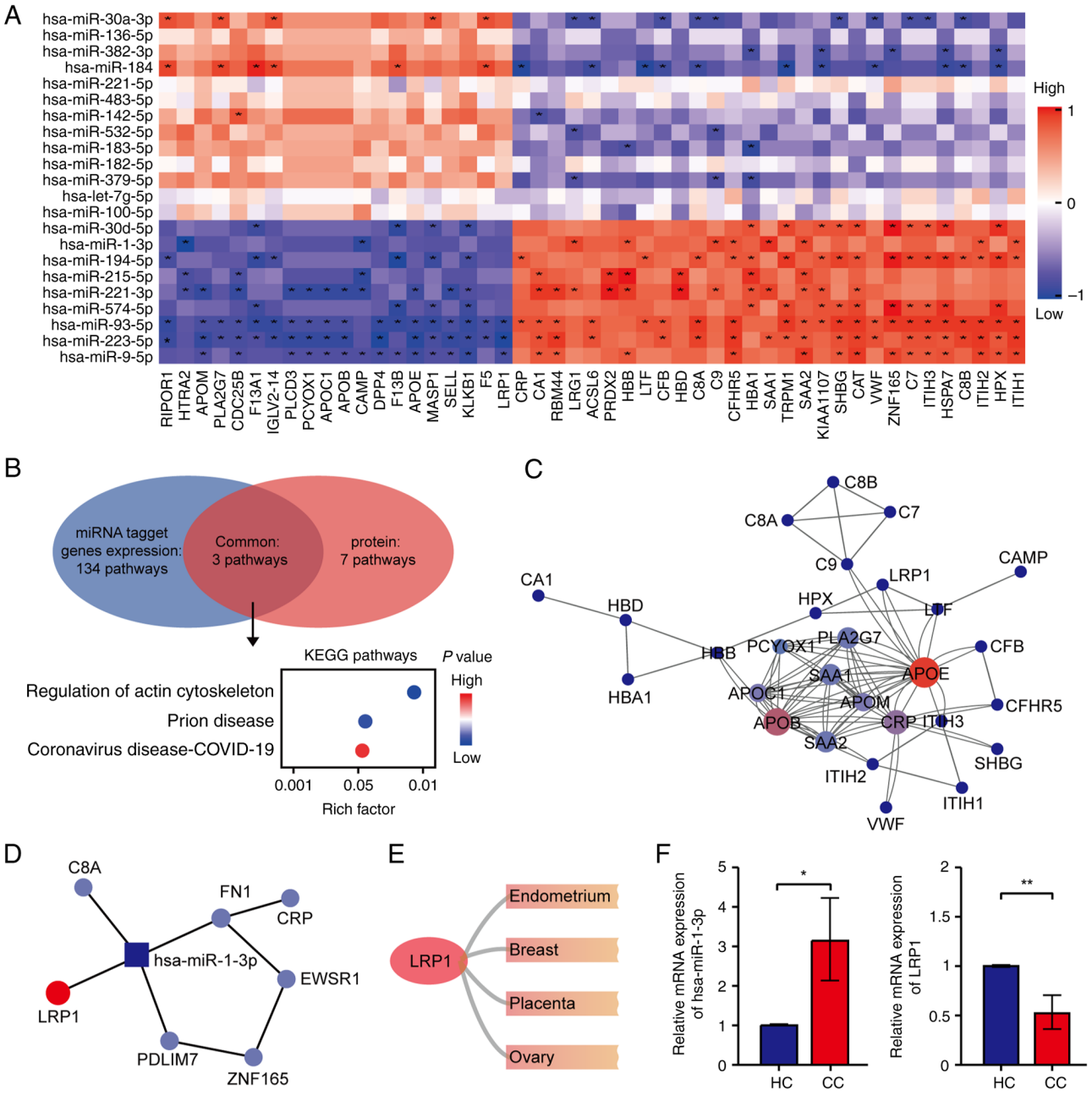

Figure 4. Integrated analysis of EV-derived miRNA and proteomic data reveals a key hsa-miR-1-3p-LRP1 regulatory axis in CC. (A) Heatmap showing Spearman correlation between differentially expressed miRNAs and proteins (red: positive correlation; blue: negative correlation). (B) Differential miRNA target gene enrichment pathway and differential protein enrichment pathway and their shared metabolic pathways. (C) Protein-protein interaction network of DEPs. (D) Interaction network map of differentially expressed miRNAs and DEPs. (E) Tissue-specific expression profile of LRP1. (F) Reverse transcription-quantitative PCR validation of EV-derived hsa-miR-1-3p (left) and LRP1 (right) expression levels in HC and patients with CC (n=3) *P<0.05 and **P<0.01. EV, extracellular vesicle; miR or miRNA, microRNA; CC, cervical cancer; DEPs, differentially expressed proteins; HC, healthy controls; KEGG, Kyoto Encyclopedia of Genes and Genomes.

dysregulation of cholesterol metabolism-related proteins (such as APOE and APOB) coexists with the upregulation of inflammatory mediators (such as CRP and SAA1/2), revealing a vicious cycle where metabolic reprogramming and chronic inflammation mutually promote each other in CC, with EVs serving as important carriers for transmitting these signals (65,66). Importantly, the current study found that EV-derived hsa-miR-1-3p may suppress LRP1 expression, disrupt cytoskeletal stability and subsequently activate pro-invasive signaling pathways such as Wnt/β-catenin, ultimately accelerating CC metastasis. The present research strategy connecting upstream regulatory molecules with downstream functional proteins was able to construct a complete signaling cascade from cause to effect, providing a new explanatory framework for understanding the molecular mechanisms of CC.

In summary, the present study has systematically delineated the molecular landscape of plasma EVs in CC through an integrated multi-omics strategy and has proposed for the first time that hsa-miR-1-3p-LRP1 is a key regulatory axis involved in disease progression. This finding not only deepens the current understanding of CC molecular mechanisms, but also

lays a solid theoretical foundation for developing EV-based non-invasive diagnostic biomarkers and targeted therapeutic strategies.

Despite the aforementioned findings, the present study has several limitations. First, the relatively small sample size makes it difficult to accurately evaluate the dynamic changes of the hsa-miR-1-3p-LRP1 axis during CC initiation and progression, requiring validation through longitudinal studies in larger cohorts. Second, the current study primarily provides correlative evidence at the bioinformatics level; whether hsa-miR-1-3p directly targets, and regulates LRP1 and its specific biological functions need verification through functional experiments such as luciferase reporter assays or gene knockdown/overexpression. Furthermore, the mechanism of this regulatory axis in HPV-independent carcinogenesis remains to be further explored through future *in vitro* and *in vivo* models, which would be crucial for elucidating its specific value in different CC subtypes.

Acknowledgements

Not applicable.

Funding

The present study was supported by the 2024 Qinghai Provincial Clinical Key Specialty Construction Project Qinghui Health Office [grant no. (2024) 23].

Availability of data and materials

The data generated in the present study may be found in the Gene Expression Omnibus under accession number GSE310070 or at the following URL: https://www.ncbi.nlm.nih.gov/geo/query/acc.cgi?acc=GSE310070; and in the PRIDE Archive under accession number PXD071100 or at the following URL: https://www.ebi.ac.uk/pride/archive/projects/PXD071100.

Authors' contributions

LQ and RY designed the present study and contributed to the writing of the manuscript. TB, WL and XL collected clinical samples performed, clinical analysis and contributed to interpretation of data. YY and WZ were responsible for data analysis and interpretation, manuscript revision, response to reviewers' comments, and finalization of the manuscript. All authors read and approved the final version of the manuscript. LQ and RY confirm the authenticity of all raw data.

Ethics approval and consent to participate

The present study was conducted in accordance with the Declaration of Helsinki. Ethical approval (approval no. P-SL-202157) was obtained from the Ethics Committee of Qinghai University Hospital (Xining, China). All participants received written and verbal information about the study, including the right to voluntary participation and withdrawal. Written and verbal informed consent was obtained by all participants.

Patient consent for publication

Not applicable.

Competing interests

The authors declare that they have no competing interests.

References

1. Perkins RB, Wentzensen N, Guido RS and Schiffman M: Cervical cancer screening: A review. JAMA 330: 547-558, 2023.
2. Yuan Y, Cai X, Shen F and Ma F: HPV post-infection microenvironment and cervical cancer. Cancer Lett 497: 243-254, 2021.
3. De la Fuente-Hernandez MA, Alanis-Manriquez EC, Ferat-Osorio E, Rodriguez-Gonzalez A, Arriaga-Pizano L, Vazquez-Santillan K, Melendez-Zajgla J, Fragoso-Ontiveros V, Alvarez-Gomez RM and Maldonado Lagunas V: Molecular changes in adipocyte-derived stem cells during their interplay with cervical cancer cells. Cell Oncol (Dordr) 45: 85-101, 2022.
4. Bower JJ, Vance LD, Psioda M, Smith-Roe SL, Simpson DA, Ibrahim JG, Hoadley KA, Perou CM and Kaufmann WK: Patterns of cell cycle checkpoint deregulation associated with intrinsic molecular subtypes of human breast cancer cells. NPJ Breast Cancer 3: 9, 2017.
5. Liu Z, Lu Q, Zhang Z, Feng Q and Wang X: TMPRSS2 is a tumor suppressor and its downregulation promotes antitumor immunity and immunotherapy response in lung adenocarcinoma. Respir Res 25: 238, 2024.
6. Kandathil SA, Peter Truta I, Kadletz-Wanke L, Heiduschka G, Stoiber S, Kenner L, Herrmann H, Huskic H and Brkic FF: Lymphocyte-to-monocyte ratio might serve as a prognostic marker in young patients with tongue squamous cell carcinoma. J Pers Med 14: 159, 2024.
7. Zhang Y, Zhang Q, Han X, Han L, Wang T, Hu J, Li L, Ding Z, Shi X and Qian X: SLAMF8, a potential new immune checkpoint molecule, is associated with the prognosis of colorectal cancer. Transl Oncol 31: 101654, 2023.
8. Garcia J, Hurwitz HI, Sandler AB, Miles D, Coleman RL, Deurloo R and Chinot OL: Bevacizumab (Avastin®) in cancer treatment: A review of 15 years of clinical experience and future outlook. Cancer Treat Rev 86: 102017, 2020.
9. Pegtel DM and Gould SJ: Exosomes. Annu Rev Biochem 88: 487-514, 2019.
10. Quan J, Liu Q, Li P, Yang Z, Zhang Y, Zhao F and Zhu G: Mesenchymal stem cell exosome therapy: Current research status in the treatment of neurodegenerative diseases and the possibility of reversing normal brain aging. Stem Cell Res Ther 16: 76, 2025.
11. Jahan S, Mukherjee S, Ali S, Bhardwaj U, Choudhary RK, Balakrishnan S, Naseem A, Mir SA, Banawas S, Alaidarous M, *et al*: Pioneer role of extracellular vesicles as modulators of cancer initiation in progression, drug therapy, and vaccine prospects. Cells 11: 490, 2022.
12. Lee Y, Ni J, Beretov J, Wasinger VC, Graham P and Li Y: Recent advances of small extracellular vesicle biomarkers in breast cancer diagnosis and prognosis. Mol Cancer 22: 33, 2023.
13. Fang SB, Zhou ZR, Peng YQ, Liu XQ, He BX, Chen DH, Chen D and Fu QL: Plasma EVs display antigen-presenting characteristics in patients with allergic rhinitis and promote differentiation of Th2 cells. Front Immunol 12: 710372, 2021.
14. Woo HK, Park J, Ku JY, Lee CH, Sunkara V, Ha HK and Cho YK: Urine-based liquid biopsy: Non-invasive and sensitive AR-V7 detection in urinary EVs from patients with prostate cancer. Lab Chip 19: 87-97, 2018.
15. Hu L, Zhang T, Ma H, Pan Y, Wang S, Liu X, Dai X, Zheng Y, Lee LP and Liu F: Discovering the secret of diseases by incorporated tear exosomes analysis via rapid-isolation system: iTEARS. ACS Nano 16: 11720-11732, 2022.
16. Casanova-Salas I, Aguilar D, Cordoba-Terreros S, Agundez L, Brandariz J, Herranz N, Mas A, Gonzalez M, Morales-Barrera R, Sierra A, *et al*: Circulating tumor extracellular vesicles to monitor metastatic prostate cancer genomics and transcriptomic evolution. Cancer Cell 42: 1301-1312.e7, 2024.

17. Lucien F, Gustafson D, Lenassi M, Li B, Teske JJ, Boilard E, von Hohenberg KC, Falcón-Perez JM, Gualerzi A, Reale A, *et al*: MIBlood-EV: Minimal information to enhance the quality and reproducibility of blood extracellular vesicle research. J Extracell Vesicles 12: e12385, 2023.
18. Thippabhotla S, Zhong C and He M: 3D cell culture stimulates the secretion of in vivo like extracellular vesicles. Sci Rep 9: 13012, 2019.
19. Li Y, Zhao J, Yu S, Wang Z, He X, Su Y, Guo T, Sheng H, Chen J, Zheng Q, *et al*: Extracellular vesicles long RNA sequencing reveals abundant mRNA, circRNA, and lncRNA in human blood as potential biomarkers for cancer diagnosis. Clin Chem 65: 798-808, 2019.
20. Garcia-Martin R, Wang G, Brandão BB, Zanotto TM, Shah S, Kumar Patel S, Schilling B and Kahn CR: MicroRNA sequence codes for small extracellular vesicle release and cellular retention. Nature 601: 446-451, 2022.
21. Hasanzadeh M, Movahedi M, Rejali M, Maleki F, Moetamani-Ahmadi M, Seifi S, Hosseini Z, Khazaei M, Amerizadeh F, Ferns GA, *et al*: The potential prognostic and therapeutic application of tissue and circulating microRNAs in cervical cancer. J Cell Physiol 234: 1289-1294, 2019.
22. Hoshino A, Kim HS, Bojmar L, Gyan KE, Cioffi M, Hernandez J, Zambirinis CP, Rodrigues G, Molina H, Heissel S, *et al*: extracellular vesicle and particle biomarkers define multiple human cancers. Cell 182: 1044-1061.e18, 2020.
23. Blaser MC, Buffolo F, Halu A, Turner ME, Schlotter F, Higashi H, Pantano L, Clift CL, Saddic LA, Atkins SK, *et al*: Multiomics of tissue extracellular vesicles identifies unique modulators of atherosclerosis and calcific aortic valve stenosis. Circulation 148: 661-678, 2023.
24. Yuan X, Sun L, Jeske R, Nkosi D, York SB, Liu Y, Grant SC, Meckes DG Jr and Li Y: Engineering extracellular vesicles by three-dimensional dynamic culture of human mesenchymal stem cells. J Extracell Vesicles 11: e12235, 2022.
25. Zhang H, Deng B, Jiang Y, *et al*: Proteomic analysis of cerebrospinal fluid exosomes derived from cerebral palsy children. Chinese Journal of Tissue Engineering Research 27: 903-908, 2023 (In Chinese). https://d.wanfangdata.com.cn/periodical/xdkf202306016.
26. Sheng J and Zhang WY: Identification of biomarkers for cervical cancer in peripheral blood lymphocytes using oligonucleotide microarrays. Chin Med J (Engl) 123: 1000-1005, 2010.
27. Saleh M, Virarkar M, Javadi S, Elsherif SB, de Castro Faria S and Bhosale P: Cervical cancer: 2018 revised international federation of gynecology and obstetrics staging system and the role of imaging. AJR Am J Roentgenol 214: 1182-1195, 2020.
28. Tian Y, Gong M, Hu Y, Liu H, Zhang W, Zhang M, Hu X, Aubert D, Zhu S, Wu L and Yan X: Quality and efficiency assessment of six extracellular vesicle isolation methods by nano-flow cytometry. J Extracell Vesicles 9: 1697028, 2020.
29. Wu T, Hu E, Xu S, Chen M, Guo P, Dai Z, Feng T, Zhou L, Tang W, Zhan L, *et al*: clusterProfiler 4.0: A universal enrichment tool for interpreting omics data. Innovation (Camb) 2: 100141, 2012.
30. Chen H and Boutros PC: VennDiagram: A package for the generation of highly-customizable Venn and Euler diagrams in R. BMC Bioinformatics 12: 35, 2011.
31. Livak KJ and Schmittgen TD: Analysis of relative gene expression data using real-time quantitative PCR and the 2(-Delta Delta C(T)) Method. Methods 25: 402-408, 2001.
32. Salib MY, Russell JHB, Stewart VR, Sudderuddin SA, Barwick TD, Rockall AG and Bharwani N: 2018 FIGO staging classification for cervical cancer: Added benefits of imaging. Radiographics 40: 1807-1822, 2020.
33. Théry C, Witwer KW, Aikawa E, Alcaraz MJ, Anderson JD, Andriantsitohaina R, Antoniou A, Arab T, Archer F, Atkin-Smith GK, *et al*: Minimal information for studies of extracellular vesicles 2018 (MISEV2018): A position statement of the international society for extracellular vesicles and update of the MISEV2014 guidelines. J Extracell Vesicles 7: 1535750, 2018.
34. Aguayo F, Perez-Dominguez F, Osorio JC, Oliva C and Calaf GM: PI3K/AKT/mTOR signaling pathway in HPV-driven head and neck carcinogenesis: Therapeutic implications. Biology (Basel) 12: 672, 2023.
35. Sacconi A, Muti P, Pulito C, Urbani G, Allegretti M, Pellini R, Mehterov N, Ben-David U, Strano S, Bossi P and Blandino G: Immunosignatures associated with TP53 status and co-mutations classify prognostically head and neck cancer patients. Mol Cancer 22: 192, 2023.
36. Khokhar M, Kartha P, Hassan S and Pandey RK: Decoding dysregulated genes, molecular pathways and microRNAs involved in cervical cancer. J Gene Med 26: e3713, 2024.
37. Cao MX, Zhang WL, Yu XH, Wu JS, Qiao XW, Huang MC, Wang K, Wu JB, Tang YJ, Jiang J, *et al*: Retraction Note: Interplay between cancer cells and M2 macrophages is necessary for miR-550a-3-5p down-regulation-mediated HPV-positive OSCC progression. J Exp Clin Cancer Res 40: 310, 2021.
38. Park D, Kim H, Kim Y and Jeoung D: miR-30a Regulates the expression of CAGE and p53 and regulates the response to anti-cancer drugs. Mol Cells 39: 299-309, 2016.
39. Bhat AA, Thapa R, Afzal O, Agrawal N, Almalki WH, Kazmi I, Alzarea SI, Altamimi ASA, Prasher P, Singh SK, *et al*: The pyroptotic role of Caspase-3/GSDME signalling pathway among various cancer: A Review. Int J Biol Macromol 242 (Pt 2): 124832, 2023.
40. Shao X, Zheng Y, Huang Y, Li G, Zou W and Shi L: Hsa-miR-221-3p promotes proliferation and migration in HER2-positive breast cancer cells by targeting LASS2 and MBD2. Histol Histopathol 37: 1099-1112, 2022.
41. Kania EE, Carvajal-Moreno J, Hernandez VA, English A, Papa JL, Shkolnikov N, Ozer HG, Yilmaz AS, Yalowich JC and Elton TS: hsa-miR-9-3p and hsa-miR-9-5p as post-transcriptional modulators of DNA topoisomerase IIα in human leukemia K562 cells with acquired resistance to etoposide. Mol Pharmacol 97: 159-170, 2020.
42. Schoen C, Glennon JC, Abghari S, Bloemen M, Aschrafi A, Carels CEL and Von den Hoff JW: Differential microRNA expression in cultured palatal fibroblasts from infants with cleft palate and controls. Eur J Orthod 40: 90-96, 2018.
43. Li M, Song J, Wang L, Wang Q, Huang Q and Mo D: Natural killer cell-related prognosis signature predicts immune response in colon cancer patients. Front Pharmacol 14: 1253169, 2023.
44. West EE, Kolev M and Kemper C: Complement and the regulation of T cell responses. Annu Rev Immunol 36: 309-338, 2018.
45. Afshar-Kharghan V: The role of the complement system in cancer. J Clin Invest 127: 780-789, 2017.
46. Loh JT, Zhang B, Teo JKH, Lai RC, Choo ABH, Lam KP and Lim SK: Mechanism for the attenuation of neutrophil and complement hyperactivity by MSC exosomes. Cytotherapy 24: 711-719, 2022.
47. Shiels MS, Katki HA, Hildesheim A, Pfeiffer RM, Engels EA, Williams M, Kemp TJ, Caporaso NE, Pinto LA and Chaturvedi AK: Circulating inflammation markers, risk of lung cancer, and utility for risk stratification. J Natl Cancer Inst 107: djv199, 2015.
48. Zhang W, Yin Y, Jiang Y, Yang Y, Wang W, Wang X, Ge Y, Liu B and Yao L: Relationship between vaginal and oral microbiome in patients of human papillomavirus (HPV) infection and cervical cancer. J Transl Med 22: 396, 2024.
49. Nadif R, Mintz M, Jedlicka A, Bertrand JP, Kleeberger SR and Kauffmann F: Association of CAT polymorphisms with catalase activity and exposure to environmental oxidative stimuli. Free Radic Res 39: 1345-1350, 2005.
50. Chen P, Zhong X, Song Y, Zhong W, Wang S, Wang J, Huang P, Niu Y, Yang W, Ding Z, *et al*: Triptolide induces apoptosis and cytoprotective autophagy by ROS accumulation via directly targeting peroxiredoxin 2 in gastric cancer cells. Cancer Lett 587: 216622, 2024.
51. Wan S, He QY, Yang Y, Liu F, Zhang X, Guo X, Niu H, Wang Y, Liu YX, Ye WL, *et al*: SPARC Stabilizes ApoE to Induce cholesterol-dependent invasion and sorafenib resistance in hepatocellular carcinoma. Cancer Res 84: 1872-1888, 2024.
52. Garcia-Arcos I, Park SS, Mai M, Alvarez-Buve R, Chow L, Cai H, Baumlin-Schmid N, Agudelo CW, Martinez J, Kim MD, *et al*: LRP1 loss in airway epithelium exacerbates smoke-induced oxidative damage and airway remodeling. J Lipid Res 63: 100185, 2022.
53. Shen S, Zhang S, Liu P, Wang J and Du H: Potential role of microRNAs in the treatment and diagnosis of cervical cancer. Cancer Genet 248-249: 25-30, 2020.
54. Song Y, Wang Z, He L, Sun F, Zhang B and Wang F: Dysregulation of pseudogenes/lncRNA-Hsa-miR-1-3p-PAICS pathway promotes the development of NSCLC. J Oncol 2022: 4714931, 2022.
55. He L, Guo Z, Wang W, Tian S and Lin R: FUT2 inhibits the EMT and metastasis of colorectal cancer by increasing LRP1 fucosylation. Cell Commun Signal 21: 63, 2023.

56. Yang Y, Mao F, Guo L, Shi J, Wu M, Cheng S and Guo W: Tumor cells derived-extracellular vesicles transfer miR-3129 to promote hepatocellular carcinoma metastasis by targeting TXNIP. Dig Liver Dis 53: 474-485, 2021.
57. Wei W and Liu C: Prognostic and predictive roles of microRNA-411 and its target STK17A in evaluating radiotherapy efficacy and their effects on cell migration and invasion via the p53 signaling pathway in cervical cancer. Mol Med Rep 21: 267-281, 2020.
58. Fu K, Zhang L, Liu R, Shi Q, Li X and Wang M: MiR-125 inhibited cervical cancer progression by regulating VEGF and PI3K/AKT signaling pathway. World J Surg Oncol 18: 115, 2020.
59. Yi Y, Liu Y, Wu W, Wu K and Zhang W: The role of miR-106p-5p in cervical cancer: From expression to molecular mechanism. Cell Death Discov 4: 36, 2018.
60. Weiss BG, Anczykowski MZ, Ihler F, Bertlich M, Spiegel JL, Haubner F, Canis M, Küffer S, Hess J, Unger K, *et al*: MicroRNA-182-5p and microRNA-205-5p as potential biomarkers for prognostic stratification of p16-positive oropharyngeal squamous cell carcinoma. Cancer Biomark 33: 331-347, 2022.
61. Babion I, Miok V, Jaspers A, Huseinovic A, Steenbergen RDM, van Wieringen WN and Wilting SM: Identification of deregulated pathways, key regulators, and novel miRNA-mRNA interactions in HPV-mediated transformation. Cancers (Basel) 12: 700, 2020.
62. Cui G, Wang L and Huang W: Circular RNA HIPK3 regulates human lens epithelial cell dysfunction by targeting the miR-221-3p/PI3K/AKT pathway in age-related cataract. Exp Eye Res 198: 108128, 2020.
63. Becker A, Thakur BK, Weiss JM, Kim HS, Peinado H and Lyden D: Extracellular vesicles in cancer: Cell-to-cell mediators of metastasis. Cancer Cell 30: 836-848, 2016.
64. Dobrolecki LE, Airhart SD, Alferez DG, Aparicio S, Behbod F, Bentires-Alj M, Brisken C, Bult CJ, Cai S, Clarke RB, *et al*: Patient-derived xenograft (PDX) models in basic and translational breast cancer research. Cancer Metastasis Rev 35: 547-573, 2016.
65. Vendrov AE, Lozhkin A, Hayami T, Levin J, Silveira Fernandes Chamon J, Abdel-Latif A, Runge MS and Madamanchi NR: Mitochondrial dysfunction and metabolic reprogramming induce macrophage pro-inflammatory phenotype switch and atherosclerosis progression in aging. Front Immunol 15: 1410832, 2024.
66. Sarwar MS, Cheng D, Peter RM, Shannar A, Chou P, Wang L, Wu R, Sargsyan D, Goedken M, Wang Y, *et al*: Metabolic rewiring and epigenetic reprogramming in leptin receptor-deficient db/db diabetic nephropathy mice. Eur J Pharmacol 953: 175866, 2023.